

Supplement of Geosci. Model Dev., 10, 1261–1289, 2017
<http://www.geosci-model-dev.net/10/1261/2017/>
doi:10.5194/gmd-10-1261-2017-supplement
© Author(s) 2017. CC Attribution 3.0 License.



Supplement of

Global methane emission estimates for 2000–2012 from CarbonTracker Europe-CH₄ v1.0

Aki Tsuruta et al.

Correspondence to: Aki Tsuruta (aki.tsuruta@fmi.fi)

The copyright of individual parts of the supplement might differ from the CC-BY 3.0 licence.

1. Sensitivity experiments of CTE-CH₄ for summer 2007

Sensitivity experiments were performed for a test period between 29 May 2007 and 30 October 2007. Summer was chosen because biospheric methane (CH₄) emissions are largest then in the Northern Hemisphere (NH), and our focus was on the northern boreal region and Europe.

5 1.1 Experimental set-up

1.1.1 EnKF parameters' sensitivity experiments

Two EnKF parameters (ensemble size and prior covariance matrix) were assessed using CTE-CH₄, with only discrete air sample observations assimilated, and prior biosphere emission estimates from the LPX-Bern. EnKF allows a full posterior probability density function of the state (scaling factor in our case) to be represented exactly by an infinite ensemble of model states. A small ensemble size is computationally cheap to apply, but it may lead to a statistical misrepresentation of the posterior distribution. Choosing the suitable number of ensembles is often a question of finding a balance between ensemble size and computational cost. For the sensitivity experiments, we used ensemble sizes of 20 (E20) and 500 (E500) members, and in addition made a specific test for degrees of freedom (d.o.f.) related to five different ensemble sizes from 20 to 500 (i.e., 20, 60, 120, 240, and 500). The Finnish Meteorological Institute (FMI) has a computer facility with 20 nodes per processor. For E20, one processor was used, and for E500, 13 processors were used. To test sensitivities of the prior distribution of the states, we carried out four E20 simulations and three E500 simulations using random initial values sampled from a normal distribution; $N(0,1)$.

A model error covariance matrix \mathbf{Q} was used to create a prior state covariance matrix at the beginning of each time step:

$$\mathbf{P}_b^{t+1} = \mathbf{P}_a^t + \mathbf{Q}, \quad (1)$$

where \mathbf{P}_b^{t+1} is the prior state covariance matrix at time $t + 1$, and \mathbf{P}_a^t is the posterior state covariance matrix at time t . Two matrices were examined in this study: identity ($\mathbf{Q1}$), and $\mathbf{Q2}$, which was based on Peters *et al.* (2005):

$$\mathbf{Q2} = \begin{pmatrix} \mathbf{A}_{IWP} & \mathbf{A}^{*1} & \mathbf{0} & \mathbf{0} & \mathbf{0} \\ \mathbf{A}^{*1} & \mathbf{A}_{WMS} & \mathbf{0} & \mathbf{0} & \mathbf{0} \\ \mathbf{0} & \mathbf{0} & \mathbf{A}_{ANT} & \mathbf{A}^{*2} & \mathbf{0} \\ \mathbf{0} & \mathbf{0} & \mathbf{A}^{*2} & \mathbf{A}_{RIC} & \mathbf{0} \\ \mathbf{0} & \mathbf{0} & \mathbf{0} & \mathbf{0} & \sigma_{ICE} \end{pmatrix},$$

$$\mathbf{A}_{kij} = \begin{pmatrix} \sigma_k^2 & \sigma_k^2 \cdot e^{-d_{ij}/L} \\ \sigma_k^2 \cdot e^{-d_{ij}/L} & \sigma_k^2 \end{pmatrix} \text{ for } k = \text{IWP, WMS, ANT, RIC},$$

where IWP (Inundated wetland and peatland), WMS (wet mineral soils), ANT (anthropogenic), and RIC (rice) are land-ecosystem types (Fig. 2 of main paper).). It was assumed that λ_{IWP} , λ_{WMS} , λ_{ANT} , λ_{RIC} , λ_{ICE} are uncorrelated, with each having a variance $\sigma_k^2 = 0.8$. Scaling factors of the same LET regions at different mTC regions (off diagonal of \mathbf{A}_{kij}) were assumed to be correlated with $\sigma_k \cdot e^{-d_{ij}/L}$, where d_{ij} is the distance between the centre of the regions (i, j), and the correlation length $L =$

900km. For mTC3 (South American tropical), 7 (Eurasian boreal), and mTC9 (Asian tropical), between λ_{IWP} and λ_{WMS} (\mathbf{A}^{*1}), and between λ_{ANT} and λ_{RIC} (\mathbf{A}^{*2}) were assumed correlated with $\sigma_k^2 \cdot e^{-d_{ij}/L}$ to constrain the emissions in those regions better. The observation network within and around these regions is particularly sparse (only one or no site in the regions), which makes it difficult to constrain the emissions in the model. For λ_{ICE} , variance σ_{ICE}^2 was set to be $1e^{-8}$ for both $\mathbf{Q1}$ and $\mathbf{Q2}$, as the emissions from this region are small, and we assumed that the prior estimates were already good.

1.1.2 Other sensitivity experiments

In the following experiments, CTE-CH₄ with an ensemble size of 500, the same set of prior state distribution sampled from the same normal distribution, $N(0,1)$ (i.e. no random error due to sampling of prior state), and $\mathbf{Q2}$ covariance were used. For sensitivity analysis, inversions were performed to examine the effects of: 1) the prior biosphere emissions by replacing the LPX-Bern emissions with the LPJ-WHyME emission estimates, 2) the observation sets by removal of continuous observations, 3) the assimilation window length by increasing it to 12 weeks instead of 5 weeks. Finally, the effect of the Tiedtke (1989) and Gregory *et al.* (2000) convection schemes in both L⁶² and L⁷⁸ configurations were examined.

1.2 Results of sensitivity experiments

1.2.1 EnKF parameters' sensitivity experiments

The results from the sensitivity runs (E20-E500) showed that the larger the ensemble size, the more stable the results were likely to be. With an ensemble size of 500, the mean estimates for the sum of biospheric and anthropogenic emissions aggregated over the test period differed by less than 0.5 Tg CH₄ between the three E500 runs (217.9 ± 28.2 , 217.7 ± 28.2 , 217.4 ± 27.3 Tg CH₄ per test period). However, with 20 ensemble members, mean estimates for the aggregated sum of biospheric and anthropogenic emissions differed by about 10 Tg CH₄ (216.7 ± 25.3 , 221.0 ± 24.9 , 224.4 ± 24.3 , 225.1 ± 24.6 Tg CH₄). The smaller posterior uncertainties in the E20 experiments than in the E500 experiments were caused by underestimation of uncertainties due to the small ensemble size. The weekly sums also showed that there were more random variations in the estimates from the E20 experiments compared to the E500 experiments (Fig. S1). The stability also depended on the available observations. Regions with dense observational networks, e.g., North American boreal, showed less variation in the estimates than regions where the observation network was sparse, e.g., Asian tropical. This held for both E20 and E500. The d.o.f. in the posterior ensembles (square of sum of singular values divided by sum of square of singular values) was small when the ensemble size was small as we cannot represent more d.o.f. than we have in the ensemble members. It increased significantly up to an ensemble size of 120, meaning the information added to the singular value decomposition matrix was significant, but the rate did not increase much after that, and slowly reached equilibrium (Fig. S2). Although we did not test larger ensemble sizes, the results suggest that 500 is large enough to represent the probability distribution well.

30 .

As expected, computational costs were higher for E500. With 13 processors of our computational system at FMI, the computational burden was about one hour of wall clock time per week of model time for E500. For E20, the burden was only about half an hour per week of model time with one processor. Note that the computational time of E500 could be as small as E20 if the number of nodes was increased to 500, i.e. using 25 processors in the FMI system. The observation operator was the most expensive, consuming about 80% of computational time for both cases.

The experiments using **Q1** and **Q2** prior covariance showed that the posterior mean emissions and their uncertainty estimates did not differ very much at a global scale. The posterior emissions that used **Q1** and **Q2** were 91 ± 14 and 91 ± 13 Tg CH₄ for biosphere emissions, and 126 ± 27 and 127 ± 26 Tg CH₄ for anthropogenic emissions (the numbers were aggregated over the entire run of 154 days), respectively. However, the regional uncertainty estimates were clearly smaller when **Q2** was used rather than **Q1**, especially in the Eurasian boreal and Asian tropical regions, and showed the effect of correlations between the nearby regions and within the region (Fig. S3). Although reduction of uncertainty does not necessarily mean the estimates were better, the experiment showed the advantage of using the more informative covariance matrix, in which logical choices for spatial error correlations are made.

1.2.2 Other sensitivity experiments

Atmospheric CH₄ mole fractions were compared to assimilated NOAA discrete air sample observations. Globally, agreement with the observations did not differ much between the inversions, i.e., CTE-CH₄ successfully optimized emissions consistent with the average global observations regardless of the setups. For European sites, variability in the posterior mole fractions was less than in the observations. For Asia temperate region, posterior mole fractions matched the observations noticeably better when the Gregory *et al.* (2000) convection scheme was used rather than the Tiedtke (1998) scheme.

Global biospheric emission estimates of LPJ-WHyME were 8 Tg CH₄ lower than those of LPX-Bern, and posterior emissions were also lower by 15 Tg CH₄ when LPJ-WHyME was used. The LPJ-WHyME estimates for Asian temperate and tropical regions were much lower than the LPX-Bern estimates, which remained the same in the posterior. In contrast, the LPJ-WHyME estimates in Eurasian boreal and northern Europe were more than twice as large as the LPX-Bern estimates, but were reduced to a level similar to the LPX-Bern estimates by inversion. The uncertainty estimates for those regions that used LPX-Bern were about a factor of three smaller, i.e., the system favoured the LPX-Bern estimates. For northern Europe, the difference in the posterior was 0.3 Tg CH₄, i.e., the inversion was not significantly sensitive to the prior estimates. For the Eurasian boreal region, the differences still remained by about 2 Tg CH₄ in the posterior, and additional observations would be needed to better constrain the estimates. The effect was also seen in the anthropogenic emissions; the posterior anthropogenic emissions were 10 Tg CH₄ greater when LPJ-WHyME was used as prior biospheric emissions. This was an effect of the inversion trying to compensate for low biosphere emissions by increasing anthropogenic emissions.

Removal of continuous observations decreased mean posterior anthropogenic emissions by about 70% in temperate North America and in southwest and east Europe. The decrease was partially compensated by an increase in biospheric emissions; for the North American temperate region, posterior biospheric emissions were about 100% larger without assimilating continuous observations, and the estimates were similar to the prior. Furthermore, the decrease was also compensated by >50% increase Asian tropic emission estimates. However, differences in biospheric emissions in the Asian temperate region were small. The reason could be that the discrete observations may have had little effect on the biospheric emissions, as the observations were located near anthropogenic sources. Therefore, the inversion less sensitive to biospheric emissions when continuous measurements are not assimilated. The effect of removing continuous observations was also significant in the uncertainty estimates, which were larger for anthropogenic emissions than for biospheric emissions. The posterior uncertainty for global anthropogenic emissions was about two times larger in the inversion not assimilating continuous observations, and the largest differences were found in the North American temperate and Asian temperate regions, and in southwest Europe. The posterior biospheric emission uncertainty was about three times larger in North American boreal, about twice as large in Asian temperate, and about 20% larger in North American temperate, Eurasian boreal, and Asian tropical regions than the estimates using continuous observations. These results indicate that improving prior estimates is important, especially for regions where observations are sparse.

When a longer assimilation window length was used, effects of observations on emission estimates extend further in time, which could be an advantage in regions where the observation network is sparse. However, the longer travel time between sources and observations also increased the transport error, and correlates transport errors across the observation network, making them less informative. Despite that, the mean and uncertainty estimates were not significantly different for both anthropogenic and biospheric emissions regardless of assimilation window length; i.e.. the expected differences were not seen in regions such as the Tropics. One reason for this would be the short test period examined, as the correlation between tropical and extratropical fluxes became significant only after several months of transport time. Simulations with longer time periods may also reveal the impacts in our model, especially in the tropics, but it may have a negative influence in other regions (Babenhauserheide *et al.*, 2015).

Total global posterior mean biospheric and anthropogenic emissions were similar regardless of the convection schemes, but the sum of the posterior mean emissions in the SH was about 10 Tg CH₄ smaller, and that in the NH was larger when the Gregory *et al.* (2000) convection scheme was used. Due to faster vertical mixing in the NH in the Gregory *et al.* (2000) convection scheme, the simulated atmospheric CH₄ mole fractions in the troposphere were lower compared to the Tiedtke (1989) convection scheme. Therefore, CTE-CH₄ produced larger emission estimates in the NH when the Gregory *et al.* (2000) convection scheme was used.

The effect of convection was generally larger when using L^{78} than L^{62} configurations. With L^{78} , posterior anthropogenic emissions differed by more than 10% in 12 mTCs due to convection, whereas the posterior anthropogenic emissions differed by more than 10% in only two mTCs with L^{62} . For biospheric emissions, the number of regions affected was similar in both models, but the magnitude of the differences was generally larger in L^{78} . The extreme cases were seen in temperate Asia and northwest Europe, where posterior mean biosphere emissions in temperate Asia were more than 70% smaller using the Gregory *et al.* (2000) scheme than using Tiedtke (1989), and posterior mean anthropogenic emissions in northwest Europe were about 45% larger when Gregory *et al.* (2000) was used. The estimates differed by about 1% and 8% in L^{62} in those regions. One reason that L^{78} had a larger influence on the convection schemes was the increase in the number of optimization regions. If a large prior biospheric emission remains in “anthropogenic regions” (RIC, ANT, WTR), the effect of convection in biospheric emission estimates in L^{78} would be larger than in L^{62} , because biospheric emissions in those regions were not optimized in L^{62} . This was the case for the Asian temperate region; prior biospheric emissions in the anthropogenic regions were about 20 Tg CH_4 (nearly 75% of the regional prior biospheric emissions). Similarly for northwest Europe, prior anthropogenic emissions in biosphere regions (IWP and WMS) were about 74% of regional total prior anthropogenic emissions.

References

- 15 Babenhauserheide, A., Basu, S., Houweling, S., Peters, W. and Butz, A.: Comparing the CarbonTracker and TM5-4DVar data assimilation systems for CO_2 surface flux inversions, *Atmos. Chem. Phys.*, 15(17), 9747–9763, doi:10.5194/acp-15-9747-2015, 2015.
- Gregory, D., Morcrette, J.-J., Jakob, C., Beljaars, A. C. M. and Stockdale, T.: Revision of convection, radiation and cloud schemes in the ECMWF integrated forecasting system, *Q.J.R. Meteorol. Soc.*, 126(566), 1685–1710, doi:10.1002/qj.49712656607, 2000.
- 20 Peters, W., Miller, J. B., Whitaker, J., Denning, A. S., Hirsch, A., Krol, M. C., Zupanski, D., Bruhwiler, L. and Tans, P. P.: An ensemble data assimilation system to estimate CO_2 surface fluxes from atmospheric trace gas observations, *J. Geophys. Res.*, 110(D24), D24304, doi:10.1029/2005JD006157, 2005.
- Tiedtke, M.: A Comprehensive Mass Flux Scheme for Cumulus Parameterization in Large-Scale Models, *Mon. Wea. Rev.*, 25 117(8), 1779–1800, doi:10.1175/1520-0493(1989)117<1779:ACMFSF>2.0.CO;2, 1989.

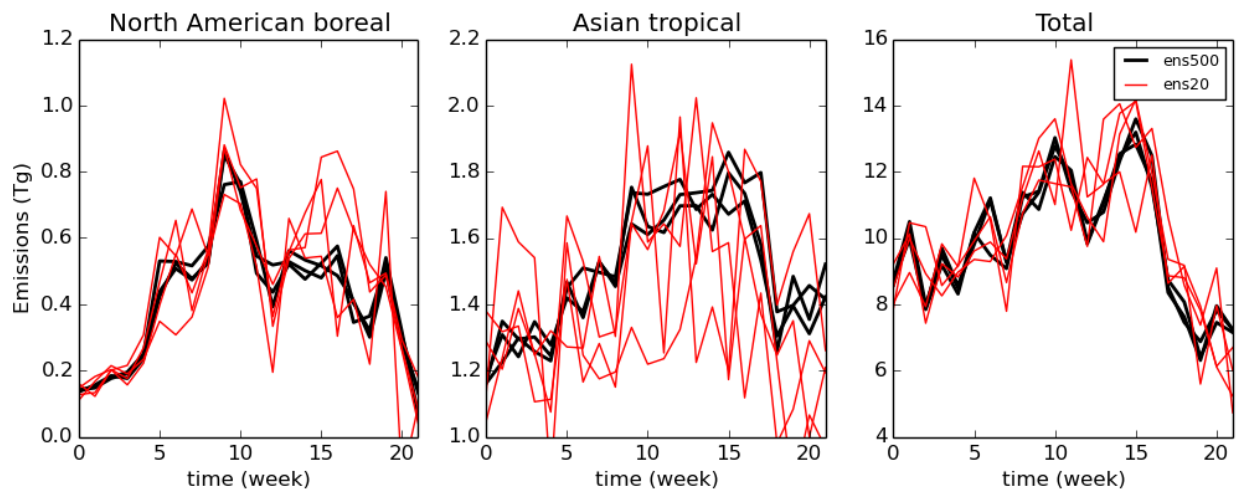


Figure S1: Weekly sum of posterior mean biospheric and anthropogenic emissions from six inversions with ensemble sizes of 500 and 20 members (three inversions for both sizes). For each line, the initial prior state vectors were sampled randomly from a normal distribution.

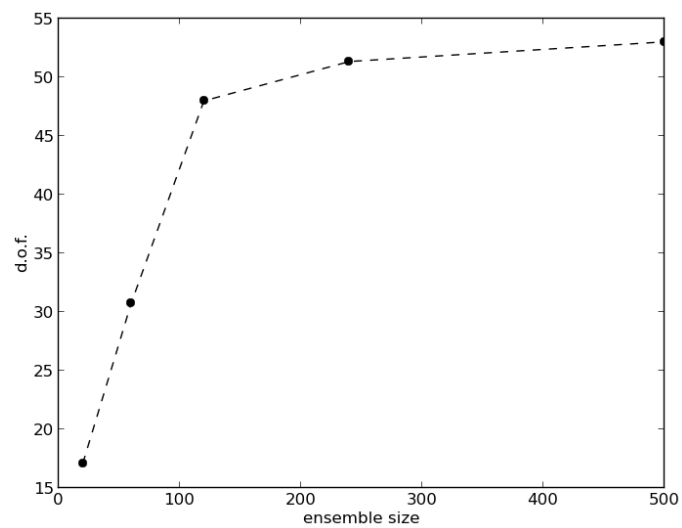


Figure S2: Number of degrees of freedom (d.o.f.) in the posterior ensemble as a function of number of ensemble.

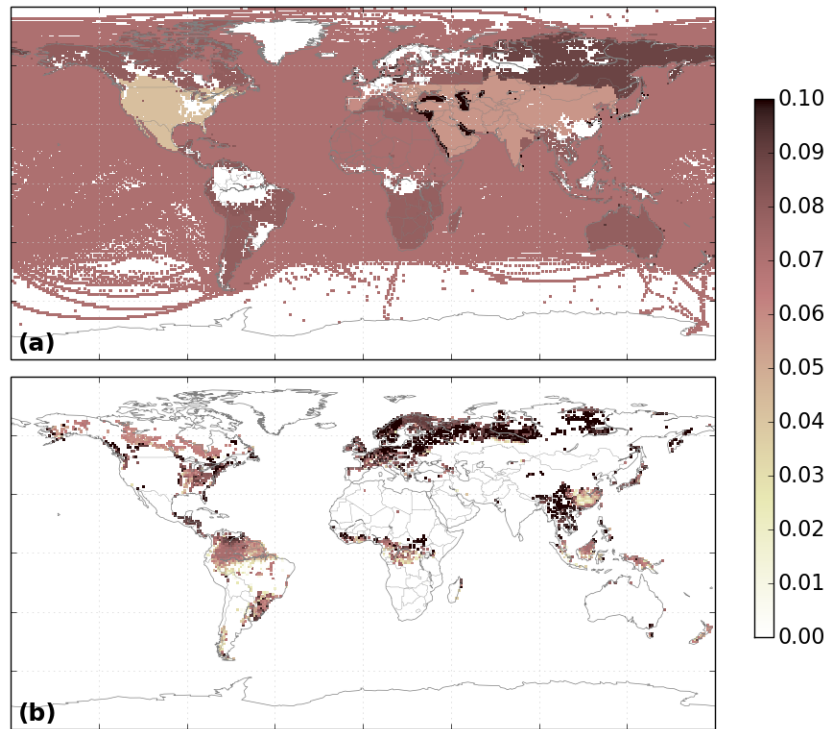


Figure S3: Relative differences in average uncertainty estimates (U) between two runs, applying covariance matrices $Q1$ and $Q2$, over the test period $(1-U_{Q2}/U_{Q1})$, for (a) anthropogenic and (b) biospheric emissions.

2. Additional materials

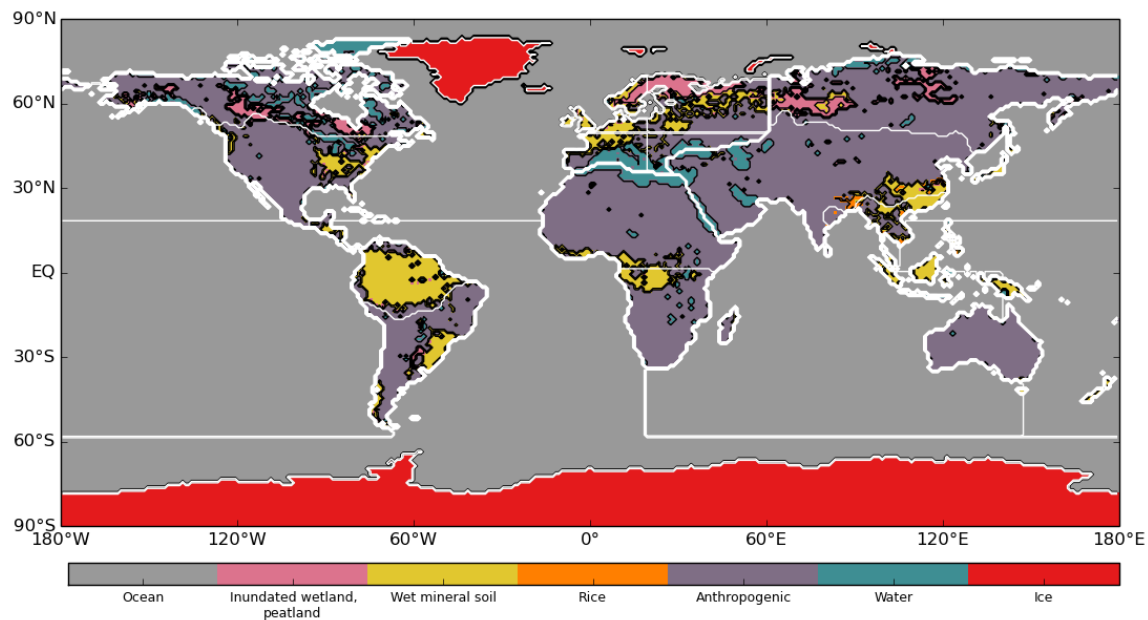


Figure S4. Land-ecosystem map used as regional definition in the optimisation. White lines illustrate mTC borders.

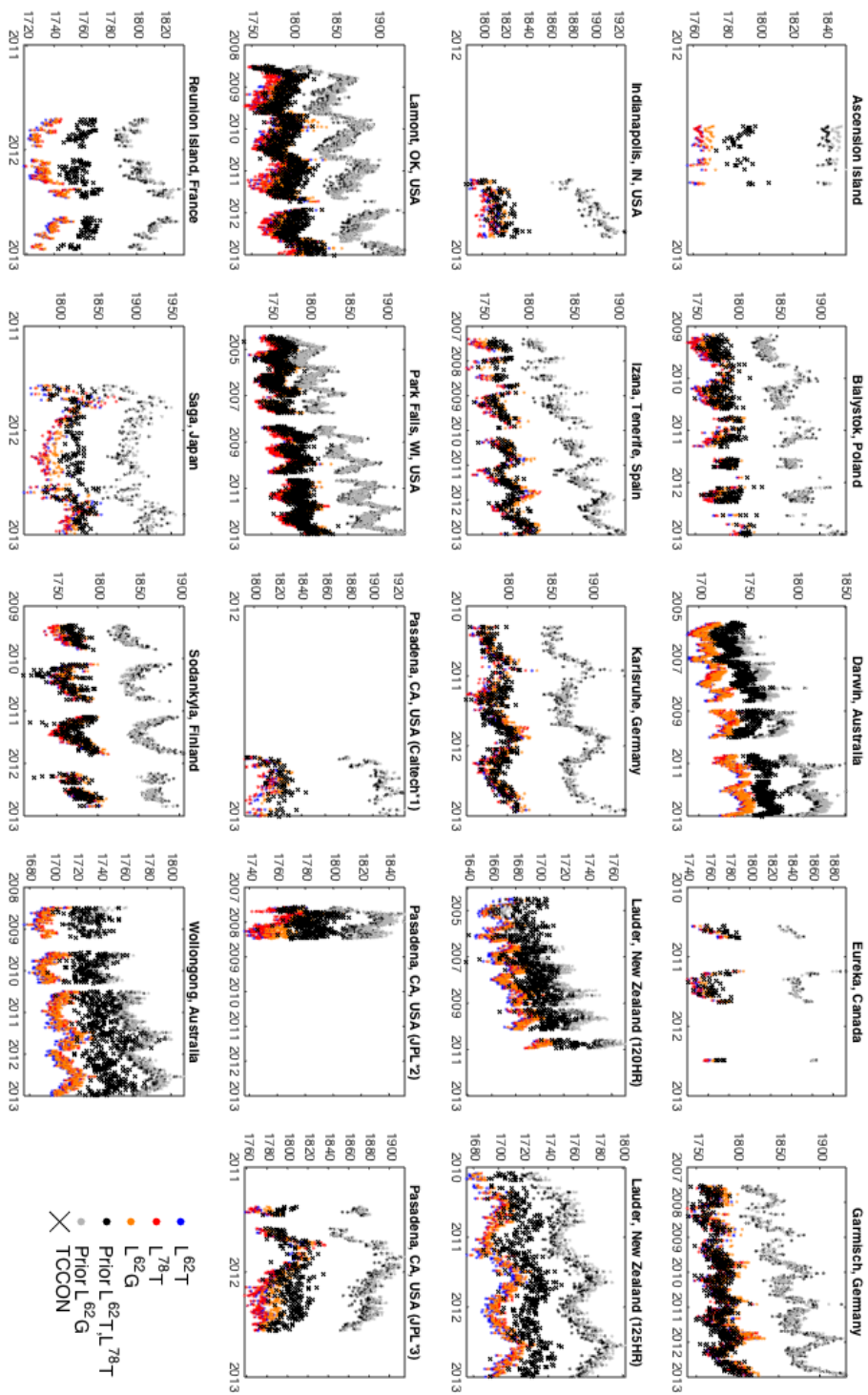


Figure S5. Observed and estimated daily mean XCH₄ at TCCON sites

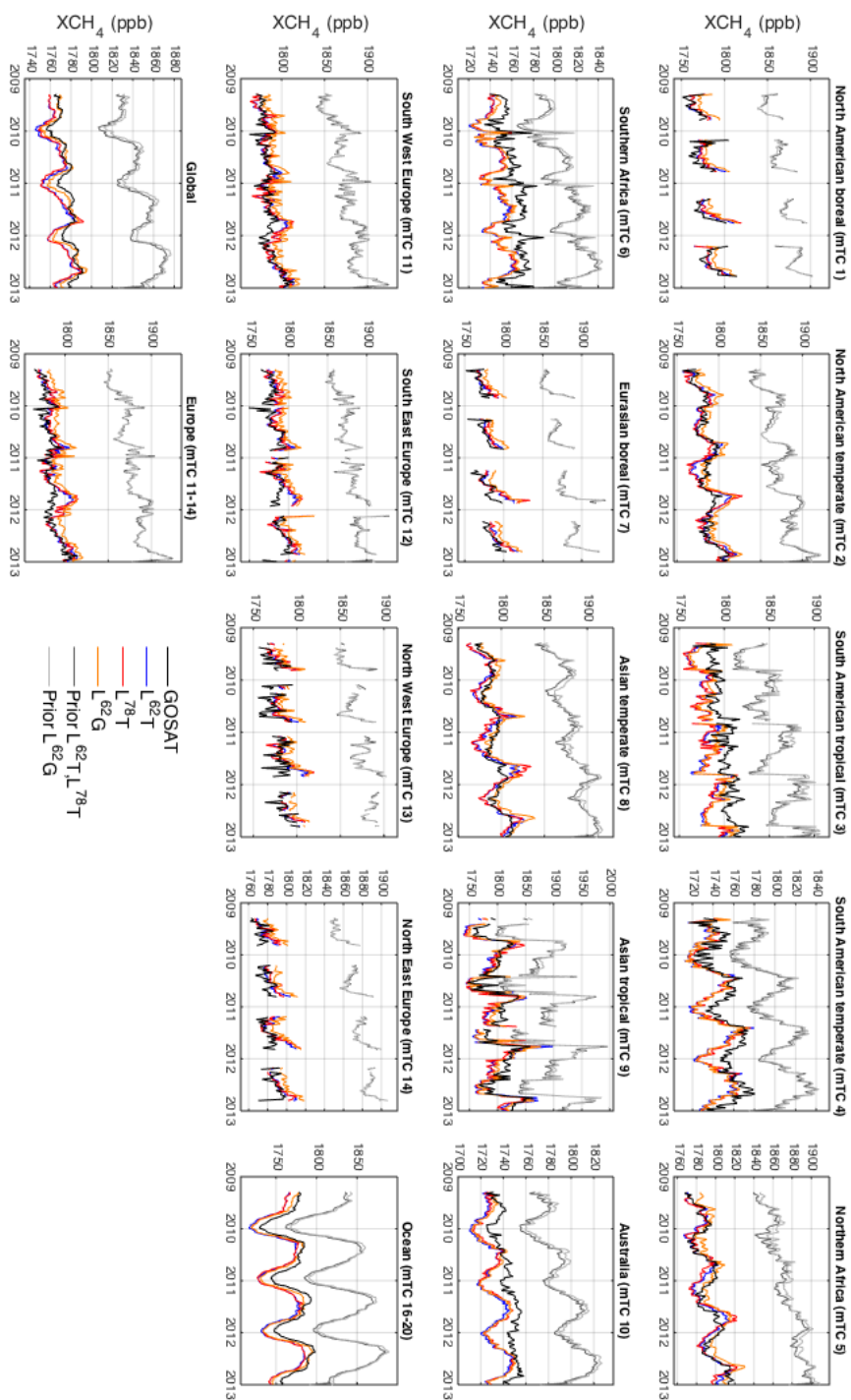


Figure S6. Global and open ocean GOSAT and simulated regional 10-day mean XCH₄.

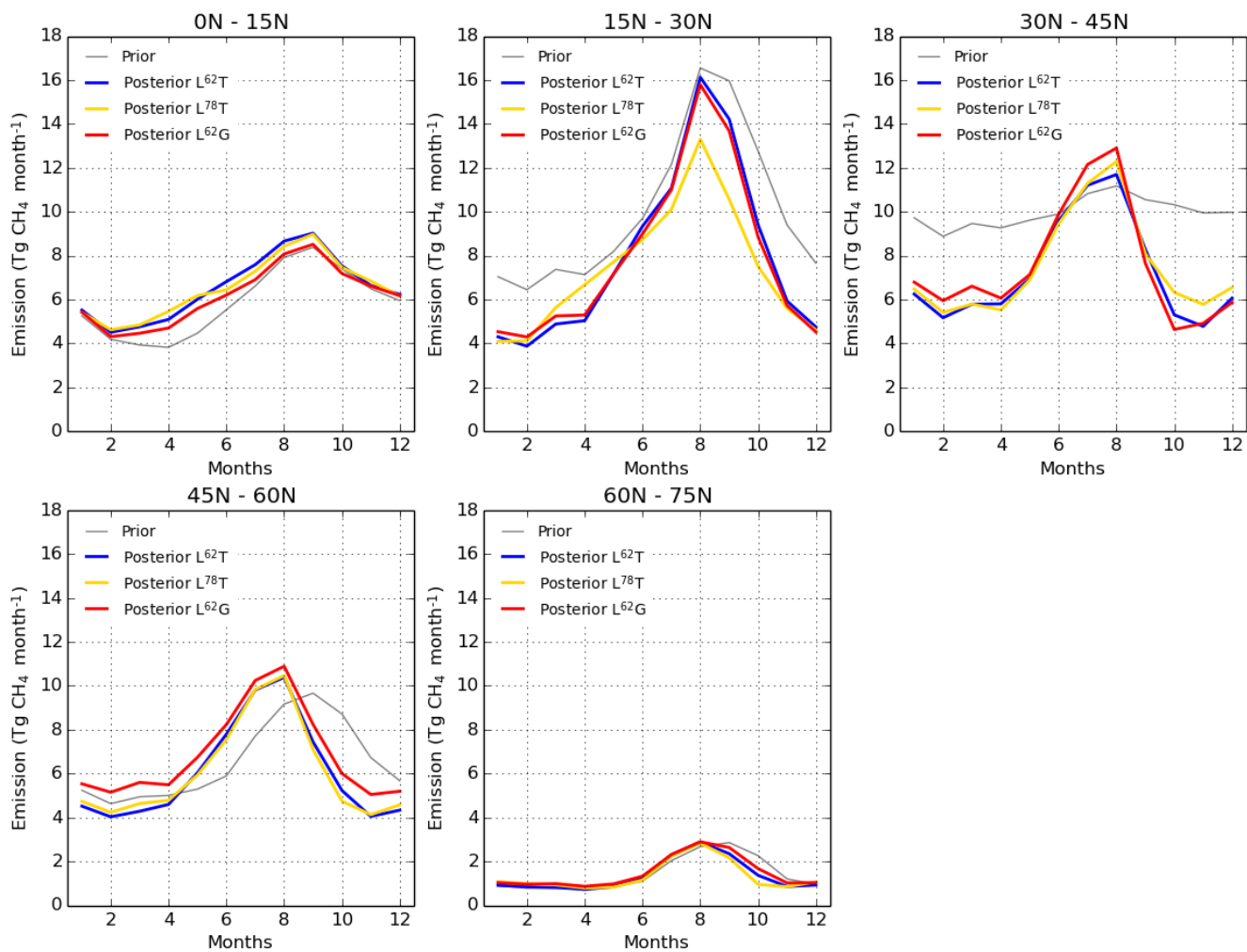


Figure S7. Monthly mean total emission estimates for different latitudinal bands, averaged over 2000-2012.

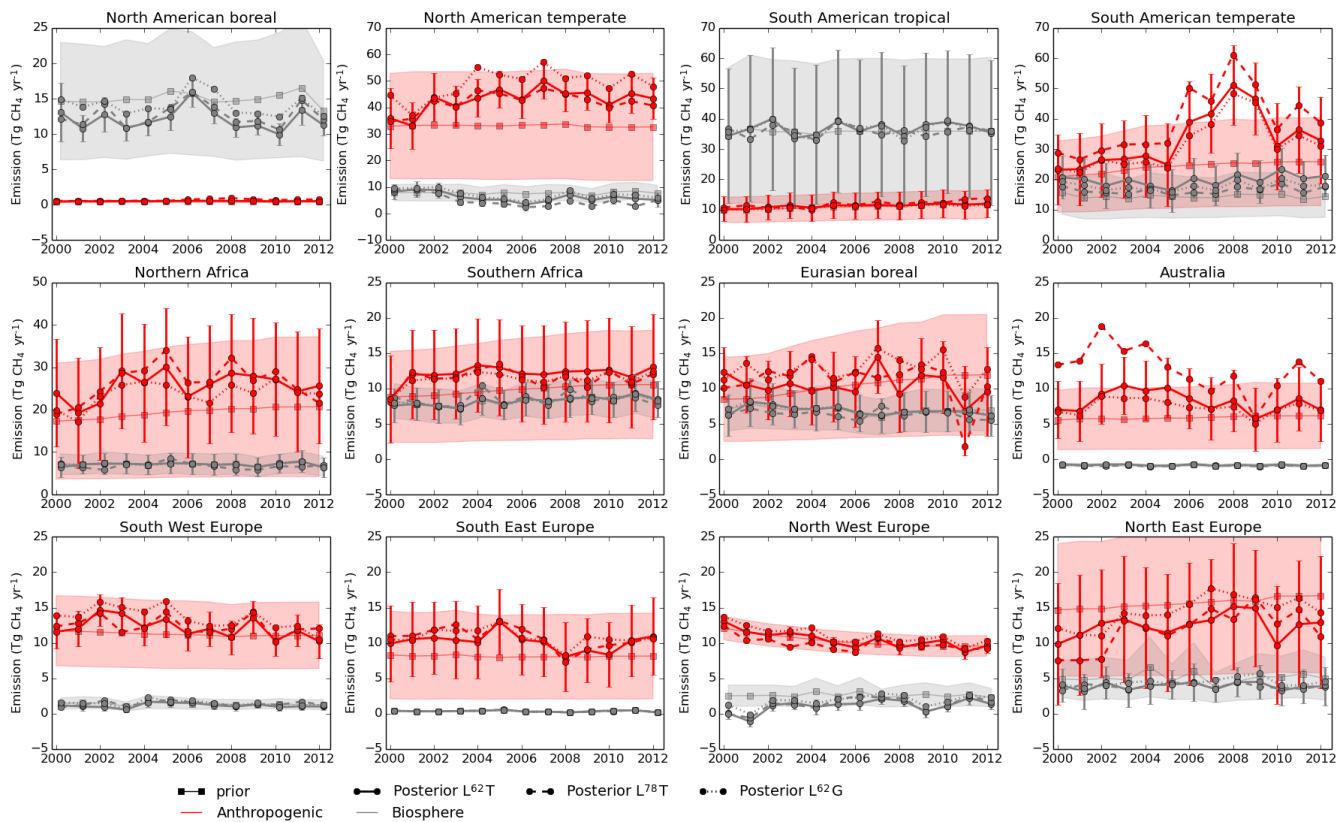


Figure S8. Regional emission estimates for land mTCs.

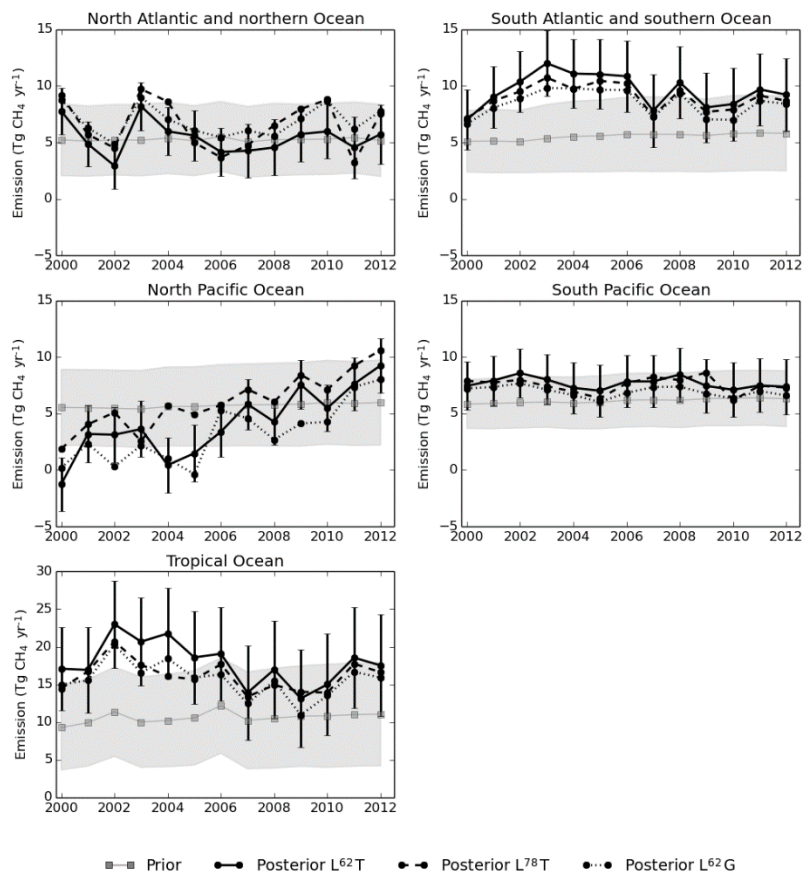


Figure S9. Regional total emission estimates for ocean mTCs.

Table S1. Mean emission estimates and their uncertainties before and after 2007 (Tg CH₄ yr⁻¹). The prior uncertainties are of L⁶²T and L⁶²G. L⁷⁸T has higher prior uncertainties in all regions due to a model feature. Region names and modified TransCom (mTC) region numbers are indicated.

Region (mTC)	Total		Anthropogenic		Biosphere	
	Before 2007	After 2007	Before 2007	After 2007	Before 2007	After 2007
Global						
Prior	532.9±86.7	566.0±102.6	313.0±80.7	350.5±97.5	172.8±31.6	171.8±31.8
L ⁶² T	507.0±45.1	526.3±43.7	287.0±36.4	314.9±34.5	172.8±28.7	167.7±28.7
L ⁷⁸ T	508.2±62.0	526.3±60.9	311.4±50.2	326.0±49.7	149.7±45.1	156.6±44.1
L ⁶² G	509.1±45.9	527.6±44.0	287.9±37.4	312.2±34.8	174.1±28.8	171.7±28.9
Europe (11-14)						
Prior	56.2±14.2	55.0±14.5	45.4±13.6	45.0±14.1	9.8±3.9	9.0±3.5
L ⁶² T	54.2±10.4	51.5±10.5	46.8±10.3	43.8±10.5	6.4±2.7	6.8±2.5
L ⁷⁸ T	53.3±13.3	53.3±13.3	45.1±13.4	45.1±13.5	7.2±3.6	7.1±3.4
L ⁶² G	59.7±10.6	58.5±10.7	50.9±10.6	49.1±10.7	7.7±2.7	8.4±2.5
North American boreal (1)						
Prior	16.4±8.3	16.1±8.4	0.5±0.2	0.5±0.2	15.1±8.3	14.9±8.4
L ⁶² T	13.7±2.0	12.8±1.5	0.5±0.2	0.5±0.2	12.4±2.0	11.6±1.5
L ⁷⁸ T	14.3±3.5	13.9±2.7	0.6±0.5	0.8±0.4	12.9±3.5	12.5±2.7
L ⁶² G	15.7±2.1	14.9±1.6	0.5±0.2	0.5±0.2	14.4±2.1	13.7±1.6
North American temperate (2)						
Prior	42.0±20.5	41.9±20.5	33.2±20.3	32.9±20.3	7.7±3.0	7.8±3.0
L ⁶² T	49.2±7.7	51.9±6.8	41.8±7.7	45.1±7.0	6.3±2.7	5.7±2.6
L ⁷⁸ T	48.4±9.2	48.1±6.8	42.2±9.4	43.1±7.3	5.1±3.7	3.8±3.5
L ⁶² G	55.6±8.4	59.1±7.5	47.4±8.4	51.3±7.7	7.2±2.7	6.6±2.7
South American tropical (3)						
Prior	52.2±24.2	53.6±24.4	10.5±4.3	11.4±4.6	35.8±23.8	35.9±23.9
L ⁶² T	53.6±23.9	55.1±24.1	11.0±4.3	11.7±4.5	36.7±23.5	37.1±23.6
L ⁷⁸ T	53.1±28.9	54.7±29.2	11.1±10.3	12.7±11.2	36.0±26.9	35.7±27.0
L ⁶² G	53.3±23.9	54.3±24.1	10.7±4.3	11.4±4.5	36.7±23.5	36.6±23.7
South American temperate (4)						
Prior	40.0±14.9	42.8±16.0	23.2±13.1	25.5±14.4	14.2±7.0	14.5±6.9
L ⁶² T	49.4±14.6	63.3±14.9	28.0±12.9	39.9±13.5	18.8±6.9	20.6±6.7
L ⁷⁸ T	51.9±24.6	66.0±24.7	33.6±22.5	46.4±23.0	15.7±9.8	16.9±9.9
L ⁶² G	46.0±14.6	58.8±15.0	26.3±12.9	37.9±13.5	17.0±6.9	18.2±6.8
Northern Africa (5)						
Prior	32.2±14.9	33.4±16.4	18.6±14.7	20.4±16.2	7.2±2.4	7.1±2.4
L ⁶² T	38.5±13.8	39.5±14.0	24.9±13.6	26.6±13.8	7.2±2.4	7.0±2.4
L ⁷⁸ T	40.6±19.5	39.2±19.0	27.2±16.9	26.8±16.6	7.0±9.8	6.4±9.4
L ⁶² G	37.2±14.0	37.3±14.2	23.6±13.7	24.4±14.0	7.2±2.4	7.0±2.4
Southern Africa (6)						
Prior	24.8±7.2	26.6±8.0	9.4±6.8	10.4±7.5	7.8±2.3	8.6±2.5
L ⁶² T	27.9±6.9	28.6±7.6	12.4±6.5	12.3±7.2	7.9±2.3	8.6±2.5
L ⁷⁸ T	28.1±12.2	27.4±13.4	12.2±8.8	11.3±9.8	8.3±8.5	8.5±9.0
L ⁶² G	27.1±7.0	27.7±7.7	11.6±6.6	11.6±7.3	7.9±2.3	8.5±2.5
Eurasian boreal (7)						
Prior	18.8±7.4	20.0±8.7	9.5±6.8	11.5±8.2	7.1±3.0	6.7±2.9
L ⁶² T	19.6±5.4	18.9±6.2	10.1±4.6	10.6±5.6	7.3±3.0	6.5±2.8

L ⁷⁸ T	20.6±9.2	18.4±9.5	12.1±7.7	10.2±8.6	6.4±5.9	6.4±5.4
L ⁶² G	22.0±5.5	21.6±6.2	12.5±4.7	13.2±5.6	7.3±3.0	6.6±2.8
Asian temperate (8)						
Prior	142.4±72.7	164.7±89.8	106.2±72.1	129.3±89.3	34.2±9.6	33.4±9.5
L ⁶² T	76.3±24.2	83.7±20.1	36.9±25.0	50.1±20.7	37.4±6.5	31.5±6.1
L ⁷⁸ T	66.8±28.7	80.6±24.2	48.4±26.6	54.8±23.2	16.4±24.7	23.8±22.5
L ⁶² G	78.2±25.2	81.0±19.9	37.8±26.1	44.2±20.6	38.5±6.9	34.8±6.4
Asian tropical (9)						
Prior	67.7±15.8	70.8±16.6	30.6±8.7	35.7±9.8	31.1±13.2	31.3±13.3
L ⁶² T	67.5±14.3	68.3±14.7	32.0±8.4	35.1±9.3	29.6±12.1	29.4±12.1
L ⁷⁸ T	69.2±27.8	67.5±28.8	32.2±23.0	32.5±24.7	31.1±19.6	31.3±19.7
L ⁶² G	63.2±14.3	65.1±14.8	29.8±8.4	32.8±9.4	27.4±12.2	28.5±12.2
Australia (10)						
Prior	7.1±4.3	7.2±4.6	5.7±4.3	6.1±4.6	-0.9±0.2	-0.9±0.2
L ⁶² T	10.6±4.2	8.4±4.4	9.1±4.2	7.3±4.4	-0.8±0.2	-0.9±0.2
L ⁷⁸ T	16.2±5.4	11.5±5.6	14.8±5.1	10.4±5.4	-0.9±1.6	-0.9±1.5
L ⁶² G	9.4±4.2	8.1±4.5	7.9±4.2	6.9±4.5	-0.8±0.2	-0.9±0.2
South West Europe (11)						
Prior	13.0±4.9	12.6±4.7	11.4±4.9	11.0±4.7	1.4±0.8	1.3±0.7
L ⁶² T	14.4±2.3	12.8±2.2	13.0±2.4	11.4±2.3	1.2±0.6	1.1±0.5
L ⁷⁸ T	14.6±2.0	13.6±2.0	12.8±2.2	12.0±2.2	1.5±1.0	1.3±0.9
L ⁶² G	16.5±2.5	13.9±2.4	14.7±2.6	12.4±2.5	1.6±0.6	1.2±0.6
South East Europe (12)						
Prior	8.8±6.1	8.7±6.0	8.1±6.1	8.1±6.0	0.4±0.1	0.3±0.1
L ⁶² T	11.6±5.1	10.1±4.9	10.9±5.1	9.5±4.9	0.4±0.1	0.3±0.1
L ⁷⁸ T	12.6±6.5	10.2±6.0	11.9±6.5	9.6±6.0	0.4±0.5	0.3±0.4
L ⁶² G	12.3±5.2	10.8±5.0	11.6±5.2	10.2±5.0	0.4±0.1	0.3±0.1
North West Europe (13)						
Prior	13.5±2.2	12.2±2.1	10.7±1.6	9.6±1.5	2.7±1.6	2.5±1.5
L ⁶² T	11.7±1.0	11.3±1.1	10.7±0.8	9.8±0.9	0.9±0.9	1.5±0.8
L ⁷⁸ T	11.0±1.3	11.4±1.6	9.7±1.6	9.7±1.9	1.2±1.4	1.7±1.3
L ⁶² G	13.1±1.0	12.7±1.1	11.4±0.8	10.4±1.0	1.6±0.9	2.2±0.9
North East Europe (14)						
Prior	20.8±10.4	21.5±11.0	15.2±9.8	16.3±10.6	5.3±3.2	4.9±2.9
L ⁶² T	16.5±8.6	17.4±8.9	12.3±8.4	13.1±8.8	3.9±2.4	3.9±2.2
L ⁷⁸ T	15.1±12.0	18.0±12.3	10.7±12.0	13.8±12.3	4.0±3.2	3.8±2.9
L ⁶² G	17.8±8.7	21.2±9.0	13.3±8.6	16.1±8.9	4.2±2.5	4.7±2.2
Ocean (16-20)						
Prior	32.9±8.6	33.9±9.2	20.1±8.6	21.6±9.2	3.7±0.0	3.7±0.0
L ⁶² T	46.3±7.7	44.2±8.4	33.5±7.7	31.9±8.4	3.7±0.0	3.7±0.0
L ⁷⁸ T	45.5±9.2	45.7±9.8	32.1±8.6	31.9±9.3	4.4±3.5	5.3±3.4
L ⁶² G	41.6±7.7	41.1±8.4	28.9±7.7	28.8±8.4	3.7±0.0	3.7±0.0
Ice (15)						
Prior	0.1±0.0	0.1±0.0	0.1±0.0	0.1±0.0	-0.0±0.0	-0.0±0.0
L ⁶² T	0.1±0.0	0.1±0.0	0.1±0.0	0.1±0.0	-0.0±0.0	-0.0±0.0
L ⁷⁸ T	0.1±0.1	0.1±0.1	0.1±0.1	0.1±0.1	-0.0±0.0	-0.0±0.0
L ⁶² G	0.1±0.0	0.1±0.0	0.1±0.0	0.1±0.0	-0.0±0.0	-0.0±0.0

Table S2. Root mean squared error (RMSE) between TCCON and posterior XCH4 without averaging kernel applied (ppb).

Site	Posterior				
	Latitude (°N)	Longitude (°E)	L ⁶² T	L ⁷⁸ T	L ⁶² G
Eureka, Canada	80.05	-86.42	8.48	8.21	10.26
Sodankylä, Finland	67.37	26.63	13.59	14.20	17.92
Bialystok, Poland	53.23	23.03	10.12	10.94	14.77
Karlsruhe, Germany	49.10	8.44	11.17	12.32	10.89
Garmisch, Germany	47.48	11.06	9.62	10.61	14.13
Park Falls, WI, USA	45.95	-90.27	11.07	11.52	14.96
Indianapolis, IN, USA	39.86	-86.00	8.00	8.67	11.89
Lamont, OK, USA	36.60	-97.49	14.37	16.69	11.11
Pasadena, CA, USA (Caltech*1)	34.14	-118.13	16.78	20.14	12.33
Pasadena, CA, USA (JPL*2)	34.12	-118.18	26.65	28.16	18.04
Pasadena, CA, USA (JPL*3)	34.12	-118.18	23.77	24.86	16.17
Saga, Japan	33.24	130.29	18.25	18.94	13.33
Izana, Tenerife, Spain	28.30	-16.50	10.84	10.87	16.62
Ascension Island	-7.92	-14.33	23.03	22.44	18.21
Darwin, Australia	-12.42	130.89	23.49	21.89	20.95
Reunion Island, France	-20.90	55.49	21.05	19.34	18.73
Wollongong, Australia	-34.41	150.88	26.84	24.36	24.46
Lauder, New Zealand (120HR)	-45.04	169.68	15.11	13.04	12.21
Lauder, New Zealand (125HR)	-45.04	169.68	15.48	13.30	13.03

*1 = California Institute of Technology, 2012

*2 = Jet Propulsion Laboratory, 2007-2008

*3 = Jet Propulsion Laboratory, 2011-2012

Table S3. Root mean squared error (RMSE) between GOSAT and model XCH₄ without averaging kernel applied (ppb).

Region (mTC) \ Inversion	Posterior		
	L ⁶² T	L ⁷⁸ T	L ⁶² G
Global (1-20)	12.5	12.5	7.2
EU (11-14)	11.5	12.0	15.9
North American boreal (1)	11.2	11.7	15.1
North American temperate (2)	10.4	11.7	11.0
South American tropical (3)	26.9	26.6	23.5
South American temperate (4)	19.5	17.9	18.2
Northern Africa (5)	9.4	11.2	7.8
Southern Africa (6)	21.7	20.8	19.6
Eurasian boreal (7)	11.8	12.6	16.8
Asian temperate (8)	12.3	13.7	9.4
Asian tropical (9)	24.8	25.6	19.0
Australia (10)	18.8	17.0	16.6
South West Europe (11)	12.7	13.1	15.3
South East Europe (12)	13.7	14.5	18.0
North West Europe (13)	15.4	16.4	19.6
North East Europe (14)	12.7	13.5	17.5
Ocean (16-20)	17.0	16.2	12.3